6 Wireless Power Transmission

6.1 Introduction

Wireless power transmission (WPT) refers to the concept of intentionally transferring power in a contactless manner aiming at powering a system located at a certain distance from the power source. There is a wide range of applications that require of devices and sensors operating in an autonomous manner, communicating with each other and providing us with useful information. Some of these applications include biomedical implants that require of recharging, devices placed in inaccessible locations, and the high number of sensors and devices necessary to implement the concepts of the Internet of Things and machine-to-machine communications. Wireless power transmission appears as an attractive solution to provide the required energy autonomy in these applications.

In a wireless power transmission system, a power source converts dc electrical power P_i to an RF signal P_t that is transmitted wirelessly to a target device, which receives the RF signal P_r and converts it back to dc electrical power P_L, in order to power itself. The target device harvests electromagnetic energy. The overall efficiency of such a system is defined as

$$\eta = \eta_{dcRF} \cdot \eta_{ap} \cdot \eta_{RFdc} \tag{6.1}$$

with

$$\eta_{dcRF} = \frac{P_t}{P_i} \tag{6.2}$$

$$\eta_{ap} = \frac{P_r}{P_t} \tag{6.3}$$

$$\eta_{RFdc} = \frac{P_L}{P_r}. \tag{6.4}$$

The first term η_{dcRF} is dominated by the efficiency of the amplifier stages of the power source. Continuous wave power amplifiers and oscillators can reach very high efficiencies, which, depending on the operating frequency and required output power, can vary from >95% in the low MHz range [116] to >70% in the low GHz range [117] and >60% in X-band [118] limited by device technology and parasitics. This chapter and Chapter 7 focus on the other two efficiency

https://doi.org/10.1017/9781139600255.007 Published online by Cambridge University Press

terms, the efficiency of the radiating apetures η_{ap} and the efficiency of the RF–dc conversion devices n_{RFdc}, the rectifiers.

These two efficiency terms are related to the classification of wireless power transmission systems in different categories in an indirect way. One may distinguish between high(er)-power wireless power transmission systems and low(er)-power RF harvesting systems. Typically, when intentional radiators are used, the RF power at the receiving devices is high. The high operating power has a strong effect on the resulting RF–dc conversion efficiency, which is also high. Such systems include high-power microwave power transmission systems such as wireless vehicle chargers and the solar power satellite concept [119]. UHF RFID systems, however, although they involve intentional RF power transmission, operate at low power levels with a sensitivity of approximately −20 dBm and for the purposes of this book are classified as RF harvesting systems, which is the focus of Chapter 7. In this book, we may loosely classify as RF harvesting systems ones where the input RF power at the terminals of the receiving antenna is approximately −20 dBm or less. In this case, as we will see in Chapter 7, the obtained RF–dc conversion efficiency η_{RFdc} is less than approximately 25%.

Wireless power transmission systems are also classified as near-field or far-field, depending on the electromagnetic field distribution of the transmitting and receiving radiators at the position of the receiving and transmitting antennas respectively, as described in the antenna literature, such as for example [120]. The field distribution has a strong effect on the operating efficiency of the radiating apertures η_{ap}. Brown [121] presents a plot of the efficiency of the radiating apertures versus a parameter τ,

$$\tau = \frac{\sqrt{A_t A_r}}{\lambda d}, \tag{6.5}$$

where A_t and A_r are the effective aperture areas of the transmitting and receiving antennas respectively, d the distance between the transmitting and receiving antennas, and λ the free space wavelength of the continuous wave transmitted RF signal. The efficiency η_{ap} has an exponential dependence on τ [122]

$$\eta_{ap} = 1 - e^{-\tau^2}, \tag{6.6}$$

shown in Figure 6.1. The well-known Friis transmission formula [120] is valid in the far-field of the radiating apertures and gives

$$P_r = P_t \frac{\lambda^2 G_t G_r}{(4\pi d)^2} = P_t \frac{A_t A_r}{(\lambda d)^2} \Rightarrow \eta_{ap} = \tau^2 \tag{6.7}$$

where the transmitting and receiving effective aperture areas are related to the transmitting and receiving antenna gain as $A_t = G_t \lambda^2/(4\pi)$ and $A_r = G_r \lambda^2/(4\pi)$ respectively. One can easily verify that the expression of the efficiency of the radiating apertures derived from the Friis transmission formula represents a first-order approximation of 6.6 for small τ. The agreement between the two expressions is good for $\tau < 0.5$, which corresponds to the Fraunhofer limit for

https://doi.org/10.1017/9781139600255.007 Published online by Cambridge University Press

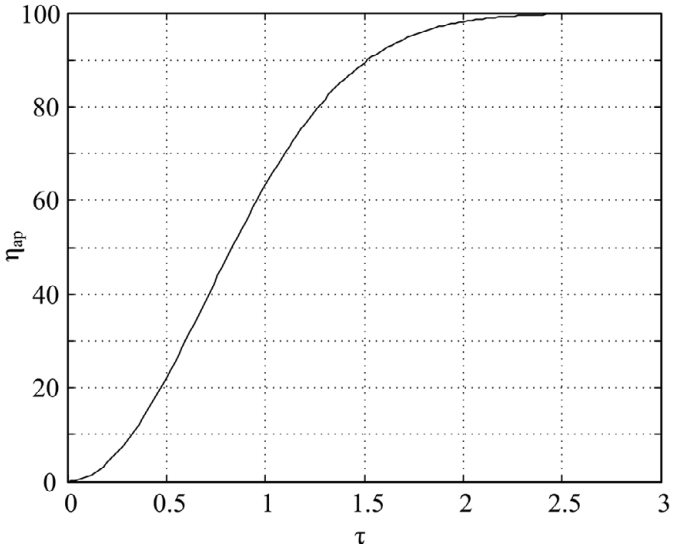

Figure 6.1 Efficiency of the radiating apertures versus τ.

the far-field [120]. As τ increases beyond 0.5, the Friis transmission formula does not apply and the system enters the near-field region. It is interesting to note that for $\tau > 2$ an efficiency of the radiating apertures of nearly 100% can be obtained.

This chapter covers near-field and far-field wireless power transmission systems, including system analysis, design guidelines, and measurement techniques. This chapter also covers, as part of near-field wireless power transmission systems, nonresonant and resonant inductive coupling covering different aspects such as impedance matching, appearing modes under strong coupling conditions, and misalignment effects. Systems employing capactive coupling are also discussed. The far-field RF/microwave radiation–based wireless power transmission section focuses on rectenna arrays for high-power transmission.

6.2 Historical Perspective

The concept of power transmission by electromagnetic waves initially appeared in the works of Hertz and Tesla [123, 124, 125]. The first wireless power transfer experiments were performed back in 1899 when Tesla tried to wirelessly transfer energy by using large coils [124, 125] at 150 KHz. Later on, W. C. Brown proposed wireless power transmission making use of higher frequencies such as microwaves in order to achieve further transmission distances [119, 126]. Toward this objective, he developed the rectenna element, comprising an antenna and a rectifier circuit connected to its terminals, which he patented in 1969 [127].

https://doi.org/10.1017/9781139600255.007 Published online by Cambridge University Press

Based on the works of Brown, the first applications of wireless power transmission focused on directive high-power transmission, such as the works on solar power satellites, appeared [119, 128, 129, 130]. Solar energy was captured and converted to electromagnetic signals that then could be reradiated and used to power devices at long distances. Recent interest in compact devices and sensors with energy harvesting capability has led some to utilize the same principle used in solar power satellites toward powering low-power electronics and sensors. As a result, low-power but highly efficient solar-to-RF converters–based solar active antennas using dc-to-RF conversion circuits such as class-E oscillators have been considered [77, 131].

Since the appearance of RF/microwave wireless power transmission, there have been a large number of works toward maximizing the power transfer efficiency in these systems mainly focusing on maximizing the RF-to-dc conversion efficiency of rectifier circuits and rectenna elements [12, 122, 132, 133, 134, 135, 136, 137, 138, 139, 140, 141, 142], synthesizing rectenna arrays for high-power wireless power transmissions [143, 144, 145, 146] and more lately there have been several efforts on the optimal transmitting signal waveform design [147, 148, 149].

On the other hand, near-field inductive coupling has also been widely studied [150, 151, 152, 153, 154, 155, 156], showing good performance from distances in the order of a few millimeters up to a couple of meters. Several methods to analyze and optimize the performance of inductive coupling systems have been used such as coupled mode theory (CMT) [150, 151, 152] and coupled inductance model circuit theory [153, 154]. CMT focuses on representing the inducting coupling system using the theory behind coupled resonators and represents the system using first-order differential equations. Circuit theory derives equations similar to the ones used in transformer circuits to describe the behavior of inductive coupling systems.

Nonresonant inductive coupling wireless power transmission has been widely used for short distances in the millimeter range and up to a few centimeters. As the targeted powering distance increases, nonresonant inductive coupling can no longer be used. Resonant inductive coupling where the transmitting and receiving coils are made to resonate by introducing additional capacitors with the adequate values allows maximizing the power transfer efficiency for the selected operating frequency. Resonant inductive coupling has been shown to achieve ranges of up to a few meters [157].

The wireless transmission of power to power up devices is pending regulation and standardization. The existing Qi standard was developed by the Wireless Power Consortium [158] and focuses on low-power (up to 5 W) inductive coupling within distances up to 40 mm. Further efforts are going on toward extending this standard to include medium power levels up to 120 W.

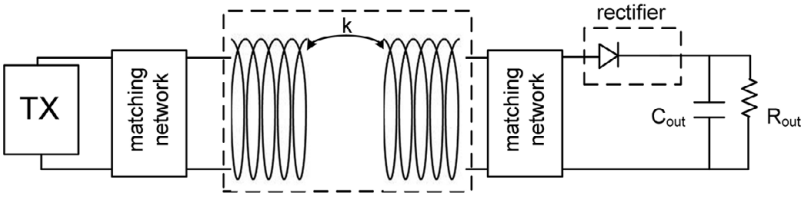

Figure 6.2 Basic building blocks of an inductive coupling wireless power transfer system.

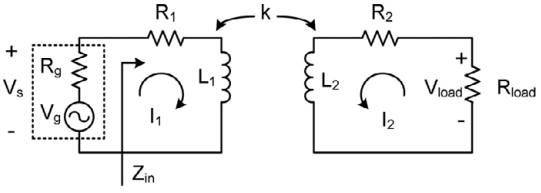

Figure 6.3 Circuit model of a nonresonant inductive coupling system.

6.3 Near-Field Wireless Power Transmission

An inductive coupling system comprises a transmitter, two inductors between which the transfer of power occurs, a rectifier circuit that converts the received power to dc and a load (Figure 6.2). Additionally, matching networks are required in the transmitting and receiving sides in order to maximize the transfer of power between the transmitter and the transmission inductor and between the receiving inductor and the rectifier circuit respectively.

6.3.1 Nonresonant Inductive Coupling

Nonresonant inductive coupling refers to the method of wirelessly transferring power by using two coupled inductors. Its working principle is based on the fact that an existing current in the transmitting coil L_1 generates a magnetic field. If the two inductors are close enough, then a change in the magnetic flux in L_1 induces a current in the receiving coil L_2. The power transfer efficiency in these nonresonant inductive coupling systems depends on several factors such as the coupling coefficient, the size of the coils, and their geometry and the alignment between transmitting and receiving coils. In order to analyze the behavior of these systems, circuit theory is used to model the power transfer process.

Figure 6.3 shows the schematic of a basic representation of a nonresonant inductive coupling system where L_1 and L_2 are the two coupled coils and R_1 and R_2 represents the internal resistances associated to L_1 and L_2.

https://doi.org/10.1017/9781139600255.007 Published online by Cambridge University Press

Applying Kirchoffs law, the equations corresponding to the circuit in Figure 6.3 can be written as follows:

$$\begin{aligned} V_s &= (R_1 + j\omega L_1)I_1 + j\omega M I_2 \\ 0 &= j\omega M I_1 + (R_2 + R_{load} + j\omega L_2)I_2. \end{aligned} \tag{6.8}$$

M is the mutual inductance among the two inductors, and it is defined as

$$M = k\sqrt{L_1 L_2}, \tag{6.9}$$

where k is the coupling coefficient among the inductors. Depending on the value of k, different types of coupling can be considered among the inductors, with $k < 0.5$ corresponding to weak coupling and $k > 0.5$ to strong coupling.

The coupling coefficient k depends of the distance between the two coils. The farther the transmitting and receiving coils are placed, the lower the value of k. In the same manner, the mutual inductance M depends on several parameters, such as the dimensions of the coils, the distance among them, and their relative position [159, 160, 161].

From (6.8), the power transfer efficiency η in a nonresonant inductive coupling system can be calculated as

$$\eta = \frac{P_{load}}{P_S} \tag{6.10}$$

with

$$\begin{aligned} P_S &= \frac{V_s I_1^*}{2} \\ P_{load} &= \frac{V_{load} I_2^*}{2} \\ V_{load} &= -I_2 R_{load}, \end{aligned} \tag{6.11}$$

where P_{load} is the average delivered power to the load, P_S is the average input power delivered at Z_{in} by the source, and the $()*$ operator indicates complex conjugate.

Using (6.8) through (6.11), one obtains

$$V_{load} = \frac{-j\omega M V_S R_{load}}{(R_2 + R_{load} + j\omega L_2)(R_1 + j\omega L_1) + \omega^2 M^2} \tag{6.12}$$

and finally

$$\eta = \frac{R_{load}}{R_2 + R_{load}} \frac{\omega^2 k^2 L_1 L_2}{[(R_2 + R_{load})^2 + (\omega L_2)^2]\frac{R_1}{R_2 + R_{load}} + \omega^2 k^2 L_1 L_2}. \tag{6.13}$$

As an example, consider a nonresonant inductive coupling circuit with $L_1 = L_2 = 10$ nH, $R_1 = R_2 = 2\ \Omega$ designed to operate at 13.56 MHz, shown in Figure 6.4. The performance of the circuit shown in Figure 6.4 in terms of power transfer efficiency can be evaluated using the preceding formulas or using a commercial simulator. Figure 6.5 shows the efficiency versus frequency for different values of the coupling coefficient k. It can be observed that this system requires a high value of k to achieve good power transfer efficiencies. As k is

https://doi.org/10.1017/9781139600255.007 Published online by Cambridge University Press

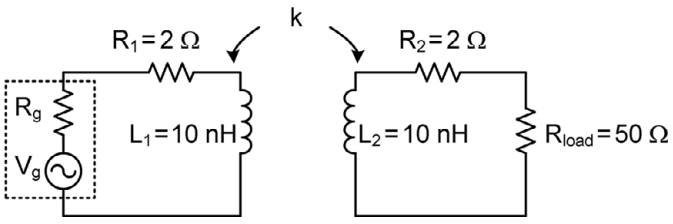

Figure 6.4 Nonresonant inductive coupling system.

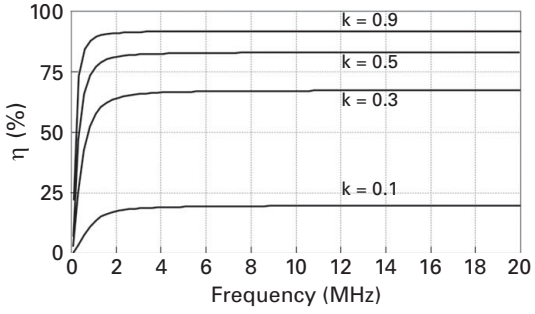

Figure 6.5 Power transfer efficiency of the nonresonant inductive coupling system of Figure 6.4.

related to the distance among the coils, this implies that the coils need to be relatively close to achieve good power transfer efficiency. This fast degradation of the power transfer efficiency with distance is the main limitation in nonresonant inductive coupling systems.

The power transfer efficiency in these systems also has a strong dependence on the value of R_{load} connected at the output of the circuit. There exists an optimum value of the load for which the power transfer efficiency is maximum. Figure 6.6 shows the power transfer efficiency versus R_{load} of the circuit of Figure 6.4 for a fixed coupling coefficient value $k = 0.1$. This result shows that the initially selected $R_{load} = 50\ \Omega$ does not lead to maximum efficiency.

6.3.2 Resonant Inductive Coupling

As stated previously, the power transfer efficiency in nonresonant inductive coupling systems degrades rapidly as the distance between the transmitting and receiving ends increases. One way to eliminate this limitation in the transfer distance is to consider resonant inductive coupling [150, 151, 152, 153, 154]. In resonant inductive coupling systems, the inductances L_1 and L_2 are made to resonate with two capacitors C_1 and C_2 introduced in the system such that both

https://doi.org/10.1017/9781139600255.007 Published online by Cambridge University Press

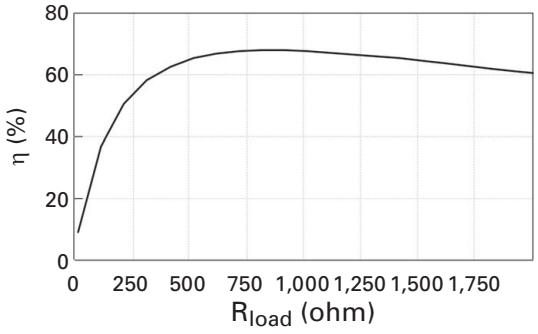

Figure 6.6 Power transfer efficiency of the nonresonant inductive coupling system in Figure 6.4 versus the output load R_{load} for a coupling coefficient of $k = 0.1$.

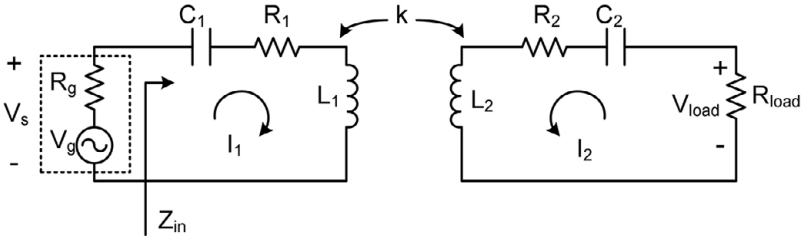

Figure 6.7 Schematic of a series–series resonant inductive coupling system.

pairs (L_1, C_1) and (L_2, C_2) resonate at the same frequency (Figure 6.7). The resonance frequencies of both resonators can be selected as

$$\omega_o = \frac{1}{\sqrt{L_1 C_1}} = \frac{1}{\sqrt{L_2 C_2}}. \tag{6.14}$$

There are four possible topologies that can be used to tune out the primary and secondary inductances, namely series–series, series–shunt, shunt–series, and shunt–shunt, shown in Figure 6.8.

The series–series topology leads to a simple mathematical analysis and will be considered next. Applying Kirchoffs law, the equations of the resonant inductive coupling system can be written as in (6.15):

$$\begin{aligned} V_s &= (R_1 + j\omega L_1 + \frac{1}{j\omega C_1})I_1 + j\omega M I_2 \\ 0 &= j\omega M I_1 + (R_2 + R_{load} + j\omega L_2 + \frac{1}{j\omega C_1})I_2. \end{aligned} \tag{6.15}$$

Using (6.11) and (6.15), the power transfer efficiency becomes as follows

$$\eta = \frac{R_{load}}{R_2 + R_{load}} \frac{\omega^2 k^2 L_1 L_2}{\left[(R_2 + R_{load})^2 + (\omega L_2 - \frac{1}{\omega C_2})^2\right] \frac{R_1}{R_2 + R_{load}} + \omega^2 k^2 L_1 L_2}. \tag{6.16}$$

https://doi.org/10.1017/9781139600255.007 Published online by Cambridge University Press

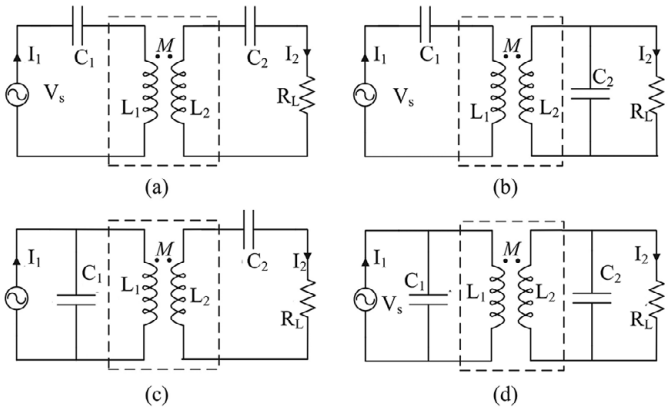

Figure 6.8 Different topologies of resonant inductive coupling systems: (a) series–series, (b) series–shunt, (c) shunt–series, and (d) shunt–shunt.

At the resonance frequency, the power transfer efficiency is maximum and can be expressed as

$$\eta_o = \frac{R_{load}}{R_2 + R_{load}} \frac{\omega^2 k^2 L_1 L_2}{R_1(R_2 + R_{load}) + \omega^2 k^2 L_1 L_2}. \tag{6.17}$$

In the same way as it happens with the nonresonant inductive coupling systems, the resonant inductive coupling system presents maximum power transfer efficiency for a certain value of R_{load} that has to be carefully selected in order to optimize the efficiency of the system.

The power transfer efficiency can also be expressed in terms of the quality factors of the inductances L_1 and L_2. Considering that the loaded quality factors of the inductances are $Q_1 = \omega L_1/R_1$ and $Q_2 = \omega L_2/R_2$ and that the quality factor of the load can be expressed as $Q_{load} = \omega L_2/R_{load}$, the power transfer efficiency expression reduces to

$$\eta_o = \frac{k^2 Q_1 Q_L}{1 + k^2 Q_1 Q_L} \frac{Q_L}{Q_{load}}, \tag{6.18}$$

where

$$Q_L = \frac{Q_{load} Q_2}{Q_{load} + Q_2} \tag{6.19}$$

is the loaded quality factor [45].

As an example, consider a resonant inductive coupling circuit with $L_1 = L_2 = 10$ nH, $R_1 = R_2 = 2\ \Omega$ designed to operate at 13.56 MHz (Figure 6.9). Capacitances C_1 and C_2 are introduced in the circuit of Figure 6.4 in order to resonate with L_1 and L_2 at 13.56 MHz. The capacitances are calculated using the expression for the resonant frequency of a resonator. In Figure 6.10, it can be seen that the power transfer efficiency of the system remains at a high value for the resonant frequency of 13.56 MHz independently of the coupling coefficient value. This shows that using a resonant inductive coupling system, it is possible

https://doi.org/10.1017/9781139600255.007 Published online by Cambridge University Press

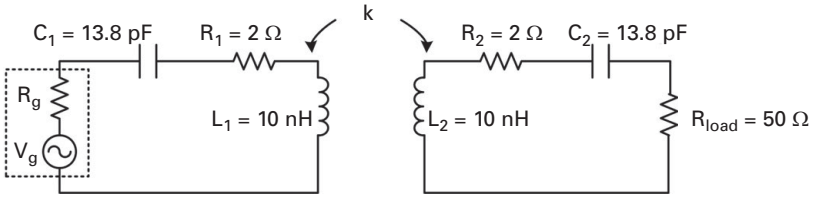

Figure 6.9 Resonant inductive coupling system example.

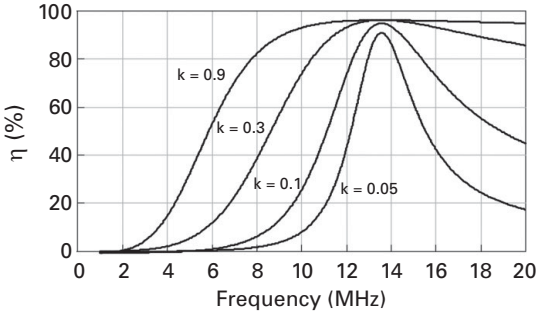

Figure 6.10 Power transfer efficiency versus frequency for different values of the coupling coefficient k.

to obtain high values of power transfer efficiency for higher distances than when using a nonresonant inductive coupling system.

6.3.3 Strong Coupling in Resonant Inductive Coupling Systems

In inductive coupling systems, additionally to the power transfer efficiency, another parameter that has to be optimized is the amount of power delivered to the load as this will determine how much dc power can be obtained when using these systems together with the RF-to-dc converter. As it can be expected, the amount of power delivered to the load depends directly on the coupling coefficient k. It could be expected that the higher the coupling coefficient k, the higher the amount of power that will be efficiently delivered to the load. This directly applies in nonresonant inductive coupling systems; however, this is not the case in resonant inductive coupling systems. Due to the coupled resonators theory, as k increases the coupling between the two inductors gets stronger and several operation modes may appear in the system. These modes produce a double peak in the output power curves around the resonance frequency, indicating that the maximum delivered power does not occur at the desired resonance frequency [154].

The location of the peaks in the output power versus frequency can be determined by calculating the derivative of P_{load} with respect to ω and setting it equal to zero as

https://doi.org/10.1017/9781139600255.007 Published online by Cambridge University Press

$$\frac{\partial P_{load}}{\partial \omega} = 0. \tag{6.20}$$

Potential ways to correct this frequency splitting effect include varying the values of C_1 and C_2 in the transmitting and the receiving ends or modifying the input/output matching networks as a manner to shift one of the peaks so that they are centered at the desired operation frequency [162].

As an example, consider the resonant inductive coupling circuit of Figure 6.9. Figure 6.11 shows the output power versus frequency for different coupling coefficient values for the circuit of Figure 6.9 that is designed to operate at 13.56 MHz. For low levels of coupling among the inductors, there is a single peak in the curve that is centered in the resonance frequency of 13.56 MHz. The output power curve begins presenting a double peak for coupling coefficient values above $k = 0.1$ (Figure 6.11b). As k continues to increase the valley between the two peaks is more pronounced and the peaks are more spaced (Figure 6.11c). When this phenomenon begins, the resonant frequency of 13.56 MHz falls in the valley between the two peaks, which means the delivered power to the load is reduced.

The second peak can be shifted back to 13.56 MHz by tuning the value of $C_1 = C_2 = C$ from the initial value of 13.8 pF to a new value of 19.5 pF. The results obtained after applying this tuning can be seen in Figure 6.12. In a similar manner, the first peak could be shifted to 13.56 MHz by tuning the value of C in the opposite direction. The applied correction may lead to reduced power transfer efficiency between the inductors, but it will improve the global performance of the system when connected to the RF-to-dc converter.

6.3.4 Impedance Matching in Inductive Coupling Systems

The power transfer efficiency calculated using (6.10) refers to the ratio between the delivered power to the load over the delivered power to Z_{in} at the input of the system of Figures 6.3 or 6.7.

The calculation of the power transfer efficiency referred to the available power at the transmitting source P_a has to take into account the mismatch between the source impedance R_g and the input impedance of the first coil Z_{in}. This efficiency can be expressed as follows

$$\eta_{av} = \frac{P_{load}}{P_a}. \tag{6.21}$$

The relationship between the delivered power P_s to Z_{in} and the available power in the source P_a can be written as

$$P_s = P_a \left[1 - |\Gamma_{in}|^2\right], \tag{6.22}$$

where Γ_{in} is the input reflection coefficient $\Gamma_{in} = (Z_{in} - R_g)/(Z_{in} + R_g)$. $Z_{in} = R_{in} + jX_{in}$ is the complex input impedance of the system. We have assumed

https://doi.org/10.1017/9781139600255.007 Published online by Cambridge University Press

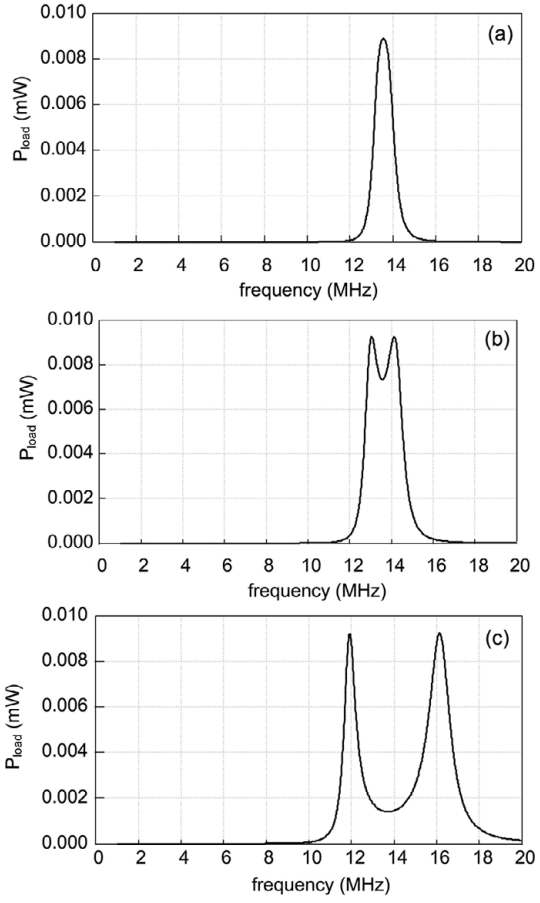

Figure 6.11 Power delivered to the load (P_{load}) versus frequency for different coupling coefficient k values (a) $k = 0.05$ (b) $k = 0.1$ (c) $k = 0.3$.

without loss of generality that the source has a real impedance R_g. Substituting (6.22) into (6.21),

$$\eta_{av} = \eta \left[1 - |\Gamma_{in}|^2\right]. \tag{6.23}$$

From (6.22), it is inferred that the maximum power transfer occurs when $|\Gamma_{in}|$ is minimum. It is straightforward to show that this occurs when $R_g = R_{in}$ and it equals $\eta_{av} = \eta$. The available maximum efficiency η_{av} represents a lower bound of the maximum efficiency η of the system.

In order to maximize the power transfer efficiency, it is important that both the source and the load are matched to the inductive coupling system. There are several ways to implement impedance matching, for example using reactive networks comprising series and parallel capacitances and inductances in different configurations in order to achieve $Z_{in} = R_g$.

https://doi.org/10.1017/9781139600255.007 Published online by Cambridge University Press

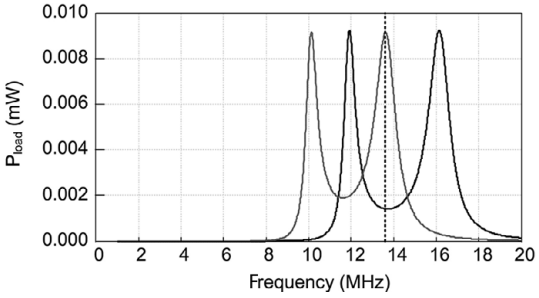

Figure 6.12 Power delivered to the load (P_{load}) versus frequency for $k = 0.3$ corrected to reach its peak value at 13.56 MHz.

6.3.5 Misalignment Effects

In the same manner as the value of the coupling coefficient k varies with distance, it is also affected by misalignments between the transmitting and receiving coils. The proper alignment of the coils in an inductive coupling system is a key parameter as the power transfer efficiency may decrease dramatically with misalignments.

Different types of misalignments may occur in an inductive coupling system (Figure 6.13):

1. Lateral misalignment: The transmitting and receiving inductors are in parallel planes but their centers are not aligned but displaced laterally a distance Δ.
2. Angular misalignment: The plane of the receiving loop is rotated by an angle θ with respect to the plane of the transmitting loop.
3. Lateral/angular misalignments: Both lateral and angular misalignments occur simultaneously.

The variation in the coupling coefficient k is due to the change in the mutual inductance between the two inductors depending on the alignment conditions. In order to estimate the variation in k, it is necessary to calculate the mutual inductance for the different alignment cases. The usual manner to solve for the mutual inductance is to use the current filament method [163, 164] that divides the cross section of the coils as a mesh of (2M + 1) by (2N + 1) for L_1 and a mesh of (2m + 1) by (2n + 1) for L_2. The mutual inductance using the filament method can be expressed as

$$M_{12} = \frac{N_1 N_2}{(2M+1)(2N+1)(2m+1)(2n+1)} \sum_j \left(\sum_i M_{ij} \right). \tag{6.24}$$

The mutual inductances M_{ij} can also be calculated using Newmanns form

$$M_{12} = \frac{\mu}{4\pi} \oint \oint \frac{dl_1 dl_2}{r_{12}}, \tag{6.25}$$

https://doi.org/10.1017/9781139600255.007 Published online by Cambridge University Press

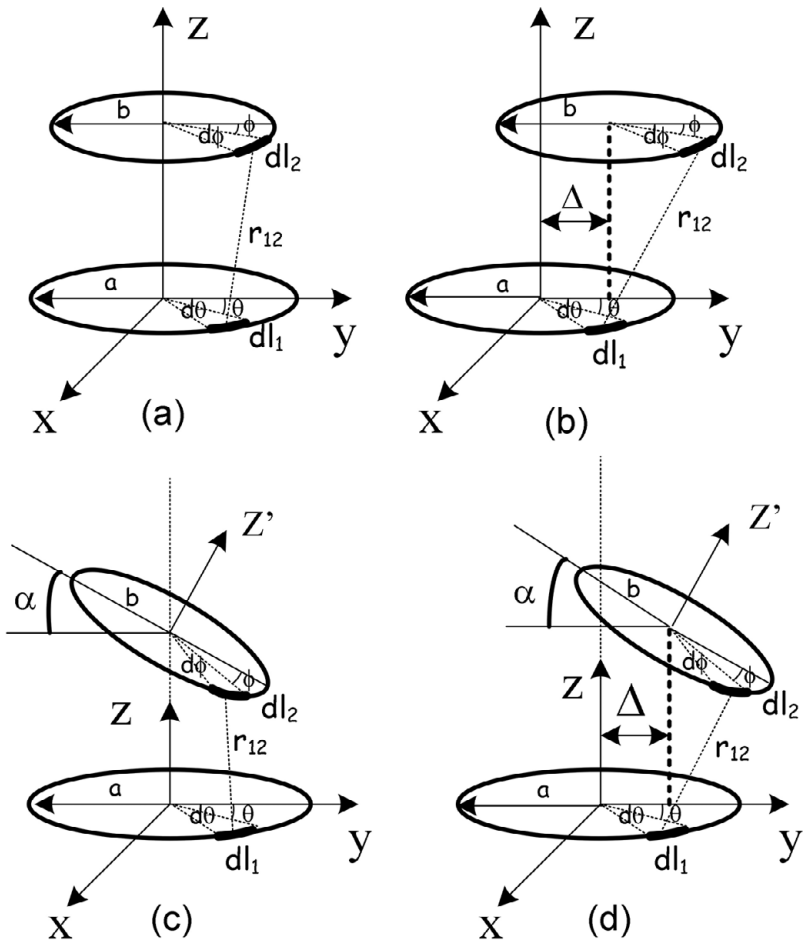

Figure 6.13 Different types of misalignments between the transmitting and receiving inductors in an inductive coupling wireless power transfer system (a) perfect alignment, (b) lateral misalignment, (c) angular misalignment, and (d) lateral and angular misalignment.

where r_{12} is the distance between the element dl_1 of coil L_1 and the element dl_2 of coil L_2.

For the aligned coil system, the distance between dl_1 and dl_2 is

$$r_{12} = \sqrt{\alpha^2 + b^2 - 2\alpha b \cos(\theta - \phi) + d^2}, \tag{6.26}$$

which results in

$$M_{12} = \mu\sqrt{\alpha b}\left[\left(\frac{2}{x} - x\right)K(x) - \frac{2}{x}E(x)\right] \tag{6.27}$$

with

$$x^2 = \frac{4\alpha b}{(\alpha + b)^2 + d^2}. \tag{6.28}$$

https://doi.org/10.1017/9781139600255.007 Published online by Cambridge University Press

$K(x)$ and $E(x)$ are the complete elliptic integrals of the first and second kind respectively that are defined as

$$K(x) = \int_0^{\pi/2} \frac{d\phi}{\sqrt{1 - x^2 \sin^2(\phi)}}$$
$$E(x) = \int_0^{\pi/2} \sqrt{1 - x^2 \sin^2(\phi)} d\phi. \tag{6.29}$$

In the case of the laterally misaligned coil system, the distance between dl_1 and dl_2 becomes

$$r_{12} = \sqrt{\alpha^2 + b^2 + 2\alpha b \cos(\theta - \phi) + 2(b - \alpha)\Delta \cos(\theta) + d^2}. \tag{6.30}$$

In the same way, the distance for the case of angular misalignment can be expressed as

$$r_{12} = \sqrt{\alpha^2 + b^2 - 2\alpha b(\cos(\theta)\cos(\phi)\cos(\alpha) + \sin(\theta)\sin(\phi)) - 2bd\cos(\phi)\sin(\alpha) + d^2}. \tag{6.31}$$

6.3.6 Measurements in Inductive Coupling Systems

There are several key parameters that need to be accurately measured when designing inductive coupling systems for wireless power transmission. The main and most common parameters include self-inductance of the inductors, mutual inductance between the inductors, quality factor of resonators when designing resonant inductive coupling systems, and power transfer efficiency. Some basic measurements guidelines are given next in order to determine these parameters.

The self-inductances L_1 and L_2 and the mutual inductance M of two coupled inductors can be obtained by measuring the impedance matrix $[Z]$ of the structure. This measurement can be done by using a conventional vector network analyzer (VNA) that allows obtaining $[Z]$ directly or by measuring the scattering parameter matrix $[S]$ and then calculating the impedance matrix $[Z]$ by using the well-known corresponding transforming relationships between $[Z]$ and $[S]$ [165].

Considering the circuit equations for a two coupled inductors structure and rearranging them in a matrix form as in (6.32) it is possible to determine L_1, L_2, and M using (6.33) through (6.36). The internal resistance of the inductors has been considered in the equations of the system (6.32).

$$\begin{bmatrix} V_1 \\ V_2 \end{bmatrix} = \begin{bmatrix} R_1 + j\omega L_1 & j\omega M \\ j\omega M & R_2 + j\omega L_2 \end{bmatrix} \cdot \begin{bmatrix} I_1 \\ I_2 \end{bmatrix} \tag{6.32}$$

$$\begin{bmatrix} Z_{11} & Z_{12} \\ Z_{21} & Z_{22} \end{bmatrix} = \begin{bmatrix} R_1 + j\omega L_1 & j\omega M \\ j\omega M. & R_2 + j\omega L_2 \end{bmatrix} \tag{6.33}$$

https://doi.org/10.1017/9781139600255.007 Published online by Cambridge University Press

$$M_{12} = M_{21} = M = \frac{\Im(Z_{12})}{\omega} = \frac{\Im(Z_{21})}{\omega} \tag{6.34}$$

$$L_1 = \frac{\Im(Z_{11})}{\omega} \tag{6.35}$$

$$L_2 = \frac{\Im(Z_{22})}{\omega}, \tag{6.36}$$

where the function $\Im()$ denotes the imaginary part of its argument.

Another parameter that needs to be determined when designing resonant inductive coupling systems is the quality factor of the resonators formed by (L_1, C_1) and (L_2, C_2) as these quality factors affect the power transfer efficiency of the system. There are several methods to measure the quality factor of resonator circuits [166, 167], such as the reflection method and the transmission method.

A way to measure the quality factor in a simple manner using scattering parameters measurement follows. The loaded quality factor can be extracted from the magnitude of S_{21} with the help of (6.37):

$$Q_L = \frac{f_o}{\Delta f}, \tag{6.37}$$

where f_o is the resonance frequency and Δf is the bandwidth at which the magnitude of S_{21} falls to half of its value or equivalently falls by 3 dB with respect to its peak value.

If it is assumed that the coupling between the resonator and the input and output networks used in the measurements setup is weak, then the following approximation for calculating the unloaded quality factor holds:

$$Q_U = \frac{Q_U}{1 - |S_{21}|^2}. \tag{6.38}$$

If the coupling of the resonator with the input and output networks is strong, then more complex methods need to be used [166, 167].

The power transfer efficiency in an inductive coupling system can also be determined by using scattering parameter measurements. The efficiency can be expressed in terms of the scattering parameters as

$$\eta = \frac{P_{load}}{P_S} = \frac{|S_{21}|^2(1 - |\Gamma_{load}|^2)}{(1 - |\Gamma_{in}|^2)|1 - S_{22}\Gamma_{load}|^2}, \tag{6.39}$$

where

$$\Gamma_{in} = \frac{S_{11} + S_{12}S_{21}\Gamma_{load}}{1 - S_{22}\Gamma_{load}}. \tag{6.40}$$

If both the input and output of the inductive coupling system are matched to the source resistance R_g and load resistance R_{load}, then $\Gamma_{in} = \Gamma_{load} = 0$ and the power transfer efficiency equation is reduced to

$$\eta = |S_{21}|^2. \tag{6.41}$$

https://doi.org/10.1017/9781139600255.007 Published online by Cambridge University Press

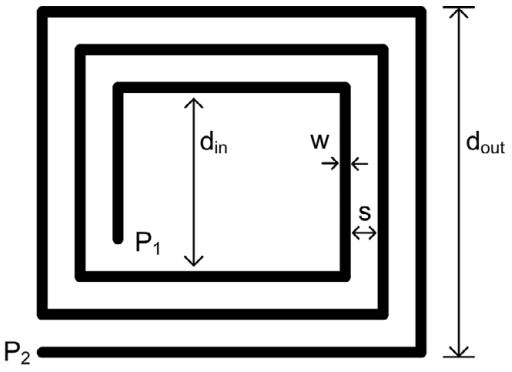

Figure 6.14 Printed inductor designed using the modified Wheeler formula.

For example, consider the design of a printed inductor on Arlon 25N substrate with $N = 3$, $w = 0.25$ mm and $s = 0.5$ mm. Depending on the geometry of the inductors that will be used for a specific design of wireless power transfer using inductive coupling, the initial dimensions of the inductors can be calculated using existing formulas and expressions [159, 160, 161, 168].

The rectangular printed inductor in Figure 6.14 has been designed using the modified Wheeler formula [160, 161], shown in (6.42), to present approximately an inductance value of $L = 0.1$ μH,

$$L = K_1 \mu_o \frac{N^2 d_m}{1 + K_2 \phi}, \tag{6.42}$$

where $\mu_o = 4\pi\dot{1}0^{-7}$ Hm^{-1} is the vacuum permeability, N is the number of turns of the inductor, K_1 and K_2 are layout-dependent parameters, and d_{in} and d_{out} refer to the inner and outer dimensions of the inductor (Figure 6.14). Finally, d_m and ϕ are defined as

$$d_m = \frac{d_{in} + d_{out}}{2} \tag{6.43}$$

$$\phi = \frac{d_{in} - d_{out}}{d_{in} + d_{out}}. \tag{6.44}$$

Assuming it is necessary to measure the inductance value of the inductor in Figure 6.14, it is possible to do so using a VNA and measuring its scattering parameters. The two ports of the inductor are marked as P_1 and P_2 in Figure 6.14. In order to measure the inductance, port P_1 is grounded and the Z-parameters are measured at P_2. If it is not possible to measure directly the Z-parameters, then one can measure Z-parameters and use the corresponding transformation relationships. The value of L can be obtained using

$$L = \frac{\Im(Z_{11})}{\omega}. \tag{6.45}$$

https://doi.org/10.1017/9781139600255.007 Published online by Cambridge University Press

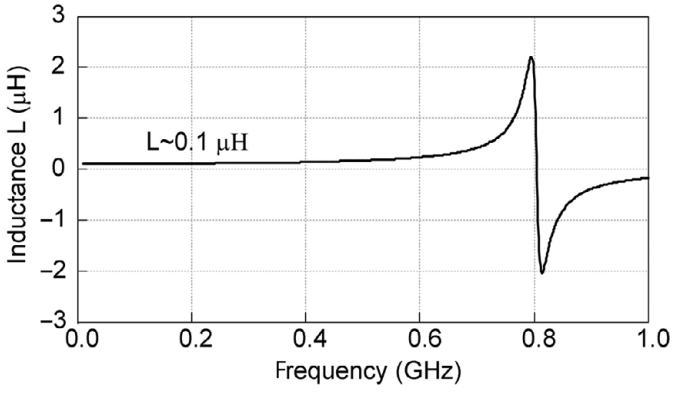

Figure 6.15 Inductance calculation from Z-parameters.

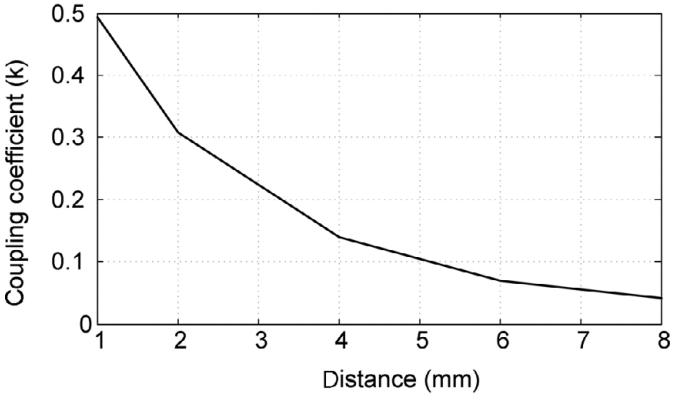

Figure 6.16 Coupling coefficient k variation with the spacing between two printed inductors as the one in Figure 6.14.

The inductance value from the printed inductor in Figure 6.14 calculated from the Z-parameters is shown in Figure 6.15. It can be observed that the obtained value is approximately $L = 0.1$ μH as it was expected. In Figure 6.15, one can observe a resonance appearing around 0.8 GHz. This self-resonance of the inductor is a consequence of its own internal capacitance.

The variation of the coupling coefficient k in a two coupled inductor system can be measured by varying the distance between the two inductors and calculating k from the measured mutual inductance M and the self-inductances L_1 and L_2 obtained from (6.34) through (6.36) using the relationship $M = k\sqrt{L_1 L_2}$. The coupling coefficient k variation versus the spacing between two inductors like the one in Figure 6.14 is shown in Figure 6.16. As expected, k decreases as the distance between inductors increases.

https://doi.org/10.1017/9781139600255.007 Published online by Cambridge University Press

6.3.7 Multiresonator Systems

As we have seen, there exist different methods to analyze and optimize the performance of inductive coupling systems, such as CMT [150, 151, 152] and coupled inductance circuit theory [153, 154]. CMT focuses on representing the inducting coupling system using the theory behind weakly coupled resonators and represents the system using first-order differential equations [152]. Circuit theory applies Kirchhoff's circuit laws to analyze the circuit behavior. In this section, we revisit the analysis of the steady state of near-field inductive coupling systems in order to determine the different operating modes, similarly to the approach followed in [169].

Let's consider first the basic resonant inductive coupling system shown in Figure 6.7. Applying Kirchoffs law and using $\omega_o = 1/\sqrt{L_1C_1} = 1/\sqrt{L_2C_2}$, the two equations representing the steady state of the system become

$$\begin{bmatrix} V_g \\ 0 \end{bmatrix} - \begin{bmatrix} R_g & 0 \\ 0 & R_L \end{bmatrix} \begin{bmatrix} I_1 \\ I_2 \end{bmatrix} = [Z] \cdot \begin{bmatrix} I_1 \\ I_2 \end{bmatrix}, \tag{6.46}$$

where

$$Z = \begin{bmatrix} R_1 + j\omega L_1 \left(1 - \frac{\omega_o^2}{\omega^2}\right) & j\omega M \\ j\omega M & R_2 + j\omega L_2 \left(1 - \frac{\omega_o^2}{\omega^2}\right) \end{bmatrix}. \tag{6.47}$$

One can rearrange (6.46) moving all resistance terms on the left-hand side resulting in

$$\begin{bmatrix} V_g \\ 0 \end{bmatrix} - \begin{bmatrix} R_g + R_1 & 0 \\ 0 & R_L + R_2 \end{bmatrix} \begin{bmatrix} I_1 \\ I_2 \end{bmatrix} = j\omega\,[X] \cdot \begin{bmatrix} I_1 \\ I_2 \end{bmatrix}, \tag{6.48}$$

where

$$X = \begin{bmatrix} L_1 & M \\ M & L_2 \end{bmatrix} - \begin{bmatrix} L_1 \frac{\omega_o^2}{\omega^2} & 0 \\ 0 & L_2 \frac{\omega_o^2}{\omega^2} \end{bmatrix} = \begin{bmatrix} L_1 & M \\ M & L_2 \end{bmatrix} - \begin{bmatrix} L_1\lambda & 0 \\ 0 & L_2\lambda \end{bmatrix} \tag{6.49}$$

and $\lambda = \omega_o^2/\omega^2$. If the input generator V_g and the losses of the system are set to zero, $j\omega X \cdot I = 0$ is a generalized eigenvalue equation defining the natural modes of the coupled inductor system. The characteristic equation is given by

$$\det X = 0 \Rightarrow \lambda^2 - 2\lambda + \left(1 - \frac{M^2}{L_1L_2}\right) = 0. \tag{6.50}$$

We have seen, however, that $M = k\sqrt{L_1L_2}$ resulting in

$$\lambda^2 - 2\lambda + \left(1 - k^2\right) = 0. \tag{6.51}$$

The two solutions of (6.51) define the two eigenvalues of the natural modes, which are equal to

$$\lambda = 1 \pm k \Rightarrow \left(\frac{\omega}{\omega_o}\right)^2 = \frac{1}{1 \pm k}. \tag{6.52}$$

https://doi.org/10.1017/9781139600255.007 Published online by Cambridge University Press

The corresponding eigenvectors become

$$\begin{bmatrix} I_1 \\ I_2 \end{bmatrix} = \sqrt{\frac{L_2}{L_1}} \begin{bmatrix} 1 \\ \pm 1 \end{bmatrix}. \tag{6.53}$$

The preceding analysis provides a mathematical description of the phenomena that was observed in Figure 6.11, where we have seen that as the coupling factor k increases the two natural modes separate in frequency. Furthermore, the currents in the two coils flow in the same or opposite directions depending on the mode. In resonant inductive coupling schemes, it is common to use multiloop structures comprising intermediate relay coils. Systems with three or four coils are commonly found in the literature [150, 153, 154, 169].

It is interesting to investigate the modes of a three coupled coil system. Following the same approach as for the two coil system, it is straightforward to find

$$X = \begin{bmatrix} L_1 & M_{12} & M_{13} \\ M_{23} & L_2 & M_{23} \\ M_{13} & M_{12} & L_3 \end{bmatrix} - \begin{bmatrix} L_1\lambda & 0 & 0 \\ 0 & L_2\lambda & 0 \\ 0 & 0 & L_3\lambda \end{bmatrix}. \tag{6.54}$$

The characteristic equation becomes a third-order polynomial, which is equal to

$$(1-\lambda)^3 - (1-\lambda)(k_{23}^2 + k_{12}^2 + k_{13}^2) + 2k_{12}k_{23}k_{13} = 0, \tag{6.55}$$

where $M_{ij} = k_{ij}\sqrt{L_i L_j}$ was used. Since the coupling factors are $k_{ij} < 1$, the rightmost term of (6.55) being a product of three coupling factors maybe considered approximately zero, which allows one to easily obtain an approximate solution for the natural modes of the system. In this case, one can see that $\lambda = 1 \Rightarrow \omega = \omega_o$ is one solution of (6.55) and therefore in the system of three coils the frequency of one of the natural modes is approximately independent of the coupling factors of the coils. This solution is exact in the case where at least one pair of the coils is uncoupled, i.e., when at least one of k_{12}, k_{23}, or k_{13} is zero. This is for example the case where two of the coils are placed far from each other and the third one is used as a relay placed in a position between the other two coils. This is an interesting result because the frequency of this mode remains constant as the distance between the coils changes, which makes the design of such a system very attractive. It is left as an exercise to the reader to find a solution for the three natural modes as a perturbation of the solution corresponding to the one obtained by ignoring the last term of the characteristic equation.

The use of relay resonators placed in intermediate locations between the transmit and receive resonators provides a natural way to increase the transmission range of the system. In [170], for example, a vision of a multiresonator space where power can be coupled to a multitude of devices exploring one or more relay resonators placed around the walls of a space is presented, shown in Figure 6.17. Metamaterial arrays of resonators may also be used as lenses in order to relay power between two resonators with increased efficiency [171]. An experimental

https://doi.org/10.1017/9781139600255.007 Published online by Cambridge University Press

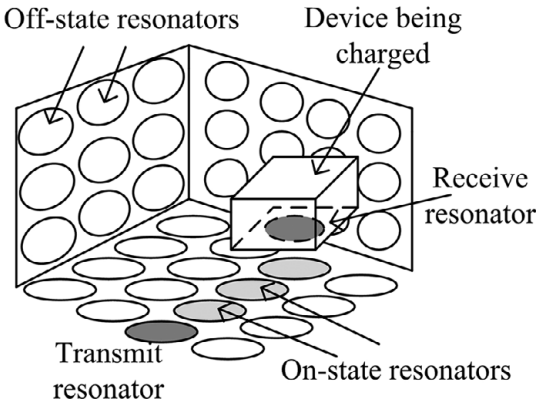

Figure 6.17 System concept of any-hop wireless power transmission.

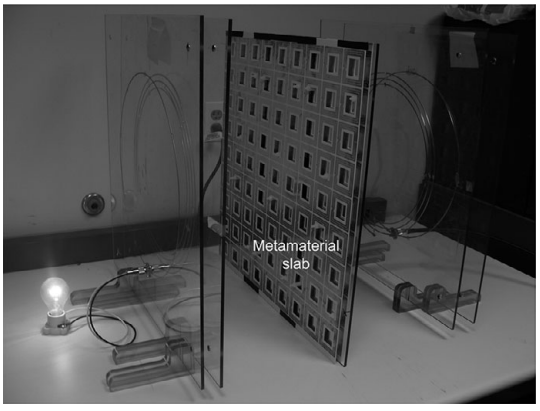

Figure 6.18 Metamaterial slab used to increase wireless power transmission efficiency of a resonant inductive coupling system demonstrator used to power a 40 W light bulb [171]. Photo courtesy of Dr. Bingnan Wang, Mitsubishi Electric Research Laboratories (MERL)

demonstrzation of a metamaterial slab used to focus the transmitted power of a resonant inductive wireless power transfer system is shown in Figure 6.18. The presence of the slab focuses the power toward the receiver, which is demonstrated by a larger intensity in the lightbulb.

Furthermore, the efficiency can be optimized by employing phased array concepts with multiple transmitters and receivers. The mathematical description of a multiple transmitter system optimization was formulated as a convex optimization problem in [156]. Convex optimization principles allow one to solve the underlying problem in an efficient and fast manner and facilitate the implementation of optimization algorithms in practical and commercial systems.

It is common to use four-loop structures such as the one shown in Figure 6.19a where two parasitic transmitting and receiving coil loops are used between the

https://doi.org/10.1017/9781139600255.007 Published online by Cambridge University Press

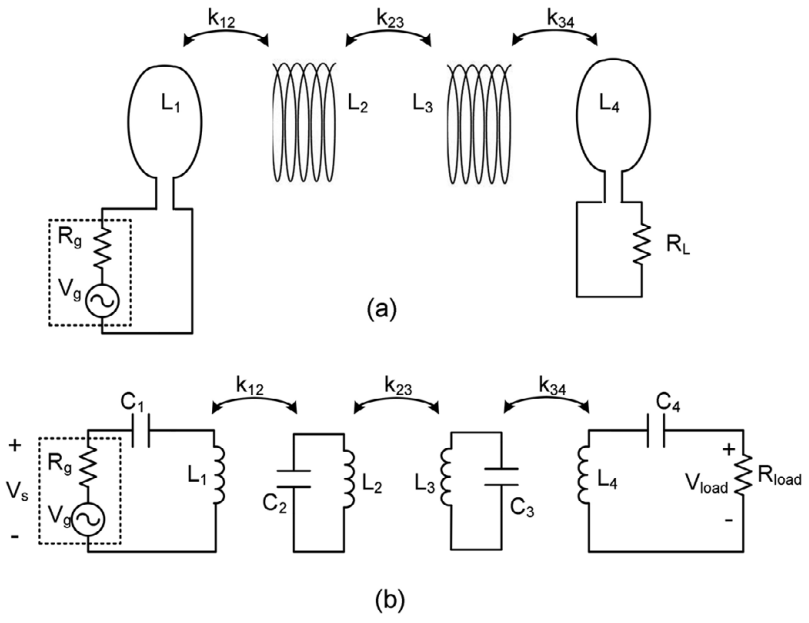

Figure 6.19 Resonant inductive coupling system with excitation loop and a load loop: (a) general scheme and (b) circuit model.

source and load loops [154]. This system has four natural modes that can be calculated following the previously descrbied methodology [169]. The two middle coils are designed to resonate at the same frequency as the transmitting and receiving coils, and they allow flexibility in implementing impedance matching for both the transmit and receive coils and maximizing the power transfer efficiency. For a fixed set of parameters of the resonant inductive coupling system, it is possible to select a coupling coefficient k_{12} between the source loop and the transmitting coil and a coupling coefficient k_{34} between the receiving coil and the load loop that allows one to optimize the input and output impedance matching conditions. The equivalent circuit model for the system in Figure 6.19a assuming resonant inductive coupling is shown in Figure 6.19b.

We have seen that as the coupling increases, which can happen for example if the distance between the coupled coils is reduced, the different modes separate in frequency [154]. As a result, an originally tuned system for a certain value of coupling may operate at a significantly reduced efficiency once the coupling changes. Alternately, an application scenario where one or both coils are moving significantly may present a large variation in operating efficiency. In order to maintain a high efficiency, one may retune the transmit or receive resonators in order to shift the operating mode frequency to a desired value that corresponds to a high efficiency. This unavoidably leads to an increased complexity in the wireless power transfer system because one needs to introduce a sensing mechanism

https://doi.org/10.1017/9781139600255.007 Published online by Cambridge University Press

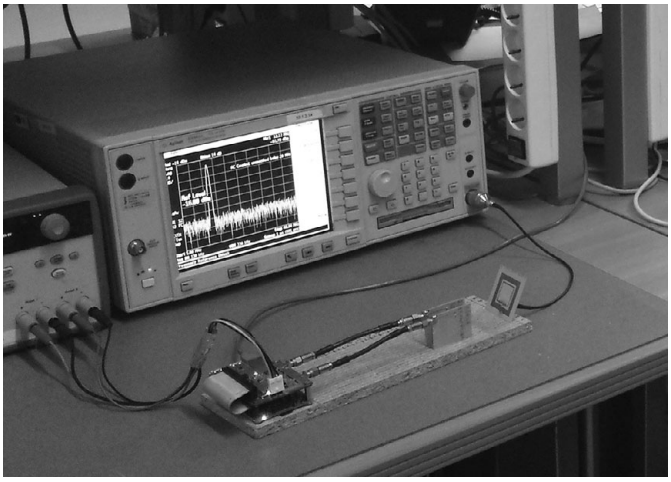

Figure 6.20 Software-defined configurable resonant inductive wireless power transfer platform based on a particle swarm optimizer (PSO) [174].

that tracks the operating efficiency, a feedback or feed forward link that can provide to the transmitter or receiver information about the efficiency and a tuning resonator functionality and control circuitry in order to implement the desired frequency tuning. Such tuning as well-adaptive tuning of wireless power transfer efficiency has received significant attention in the literature, for example in [172, 173]. In [174], for example, a software-defined radio (SDR) platform based on a Raspberry B+ evaluation module was used to implement a tunable 13.56 MHz resonant inductive wireless power transfer system, as shown in Figure 6.20. A tunable capacitor bank was controlled by the SDR platform in order to change the resonance frequency of the system based on the results of a particle swarm optimization (PSO), which was implemented offline in a Matlab environment.

6.4 Capacitive Power Transfer

An alternative way of using the magnetic field in order to transfer power wirelessly is to use the electric field. This is known as capacitive power transfer. A typical block diagram of a capacitive power transfer system is shown in Figure 6.21 [175]. In fact, Figure 6.21 shows a circuit topology of a resonant capacitively coupled system where the reactance of the coupled capacitors C_1 and C_2 has been compensated by the inductors L_1 and L_2. Similarly to the inductive coupled systems, there exist four different topologies corresponding to a parallel or series connection of the compensating inductors at the primary and secondary circuit. In practice, in addition to the two main capacitances there exist cross-coupling parasitic capacitances C_3 and C_4, as shown in Figure 6.21. One may transform the complicated coupled capacitor circuit with the parasitic capacitances into a

https://doi.org/10.1017/9781139600255.007 Published online by Cambridge University Press

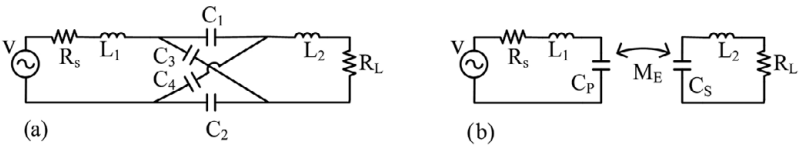

Figure 6.21 Resonant capacitive coupled wireless power transfer system: (a) circuit *schematic and (b) equivalent circuit.

circuit comprising two coupled capacitances C_P and C_S and at the same time define a capacitive mutual coupling coefficient M_E in a complete analogy with the inductive coupled systems. The resulting circuit capacitances and coupling coefficient are defined as follows [175]:

$$C_P = \frac{(C_1 + C_3)(C_4 + C_2)}{C_1 + C_3 + C_4 + C_2} \tag{6.56}$$

$$C_S = \frac{(C_1 + C_4)(C_3 + C_2)}{C_1 + C_3 + C_4 + C_2} \tag{6.57}$$

$$M_E = \frac{-C_3C_4 + C_1C_2}{C_1 + C_3 + C_4 + C_2} \tag{6.58}$$

and

$$k_E = \frac{M_E}{\sqrt{C_P C_S}}. \tag{6.59}$$

In this case, applying Kirchhoff's current laws in the system of Figure 6.21 one has

$$\begin{bmatrix} I_g \\ 0 \end{bmatrix} - \begin{bmatrix} G_g & 0 \\ 0 & G_L \end{bmatrix} \begin{bmatrix} V_1 \\ V_2 \end{bmatrix} = [Y] \cdot \begin{bmatrix} V_1 \\ V_2 \end{bmatrix}, \tag{6.60}$$

where

$$Y = \begin{bmatrix} G_1 + j\omega C_P \left(1 - \frac{\omega_o^2}{\omega^2}\right) & j\omega M_E \\ j\omega M_E & G_2 + j\omega C_S \left(1 - \frac{\omega_o^2}{\omega^2}\right) \end{bmatrix}. \tag{6.61}$$

The resonant capacitively coupled system therefore takes a dual form to the resonant inductive system of Figure 6.8.

Capacitive wireless power transfer systems were initially perceived for low power levels and at short distances in the order of 1 mm [176]. However, it was determined that both types of systems can achieve comparable efficiencies higher than 90% at kilowatt power levels, and generally there exist no guidelines to determine which type of system is more suitable for a certain power level, gap distance, and cost [176]. However, inductive power transfer systems are difficult to implement in application scenarios where power needs to be transferred through metal barriers due to eddy current losses and requires special shields to prevent electromagnetic interference (EMI) and magnetic cores to increase the coupling factors that correspondingly increase the cost. Capacitive coupled systems do not

https://doi.org/10.1017/9781139600255.007 Published online by Cambridge University Press

require magnetic cores, and because the electric field does not require a return path, it is easier to contain it between the capacitive plates and limit EMI [177].

6.5 Far-Field Wireless Power Transmission

When the distance between the transmit and receive antennas is large relative to the effective aperture area of the antennas, the wireless power transmission system operates in the far-field regime. We have seen in the introduction that in this case the Friis transmission formula holds and the efficiency of the radiating apertures η_{ap} is proportional to the square of the parameter τ, as shown in (6.7).

Following the work of Tesla, beginning in the 1960s, several far-field wireless power transmission systems have been developed, particularly in the United States and Japan. These systems comprised highly directive antennas transmitting a microwave beam on one side and large arrays of rectennas receiving the RF power and converting it to dc electrical power on the other side. There are several publications in the literature documenting these experiments, such as [121, 126, 178].

W. C. Brown demonstrated transmission of microwave power to a tethered helicopter in 1964 at Raytheon [126]. A photo of the helicopter carrying the receiving rectenna array is shown in Figure 6.22 and a more detailed photo of the "string" rectenna array is shown in Figure 6.23. The receiving array is an array of vertical strings of diodes separated by approximately a half wavelength, covering a 4 square foot area comprising 4480 IN82G diodes. It was capable of delivering a maximum dc output power of 270 W, which was sufficient to power the helicopter rotor.

In 1968, the solar power satellite concept was proposed by Glaser [126] . It consisted of capturing the sun's energy in a geosynchronous orbit and converting it into dc electrical power using solar panels and subsequently convert it into microwave power and transmit it to earth, where it can be converted back to dc electrical power. This activity has led to a milestone experiment of far-field wireless power transmission by Brown and Dickinson's team. They were able to demonstrate transmission of a microwave beam over 1 mile at 2.388 GHz at Goldstone, California, USA, in 1975 [179]. The Venus station 26 m diameter reflector antenna was used to transmit a microwave beam of up to 450 kW of power using a klystron generator. In the receiving side, a rectenna array was used comprising 17 subarrays of 270 dipole antennas each, placed above a ground plane at roughly a quarter wave distance and GaAs diode rectifiers. A photo of the experiment is shown in Figure 6.24. The efficiency of the radiating apertures of the system was approximately $\eta_{ap} = 11.3\%$. More than 30 kW of dc electrical power was received, corresponding to a RF–dc conversion efficiency of more than $\eta_{RFdc} > 80\%$ at the receiver.

Starting from the 1980s, many far-field wireless power transmission experiments were performed in Japan [178]. In 1992, a first trial employing a phased array transmitting antenna by Kyoto University and Kobe University,

https://doi.org/10.1017/9781139600255.007 Published online by Cambridge University Press

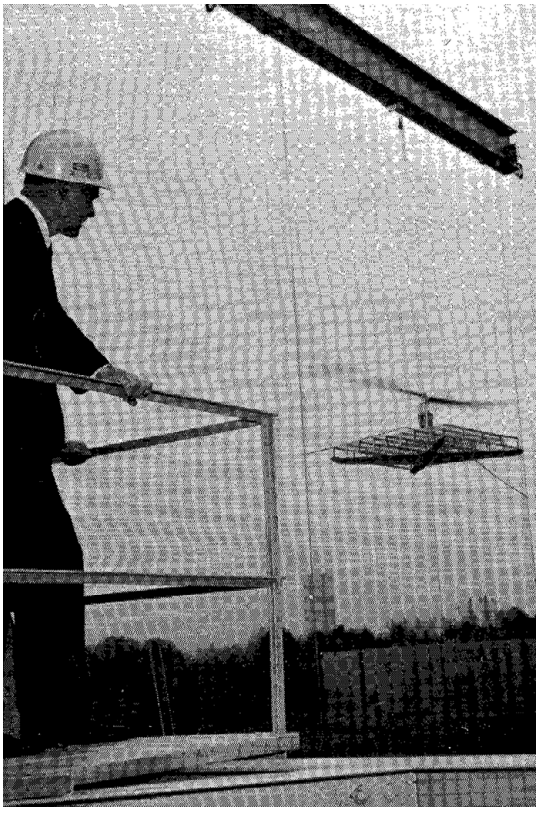

Figure 6.22 Helicopter powered by a microwave beam flying 60 ft above the transmitting antenna. ©1984 IEEE. Reprinted with permission from [126]

demonstrated flying an airplane powered by a microwave beam at 2.411 GHz using a phased array with 96 GaAs amplifiers and 288 antennas grouped in three subarrays. A photo of the airplane and the transmit phased array are shown in Figure 6.25.

Following these milestone demonstrations, a plethora of far-field wireless power transmission experiments have been performed, exploring technological advances in power generation using, for example, magnetron and solid-state amplifier arrays, exploring antenna array concepts such as retrodirective arrays as well as technological advances in devices for rectifier circuits such as GaN technology [178].

6.6 RF-to-dc Conversion: the Rectifier

In the receiving side, the received RF signal from the antenna, coil, or capacitive radiator is converted back to a dc electrical signal. A nonlinear device is necessary in order to perform frequency translation from RF to dc. Typically a nonlinear resistive element is used, such as a diode or a transistor. These nonlinear devices

https://doi.org/10.1017/9781139600255.007 Published online by Cambridge University Press

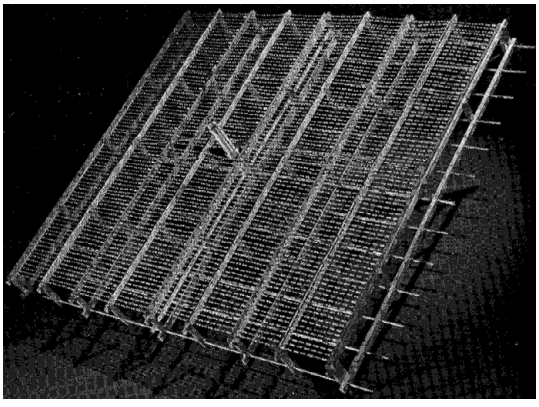

Figure 6.23 "String" rectenna used to power a helicopter in 1964. ©1984 IEEE. Reprinted with permission from [126]

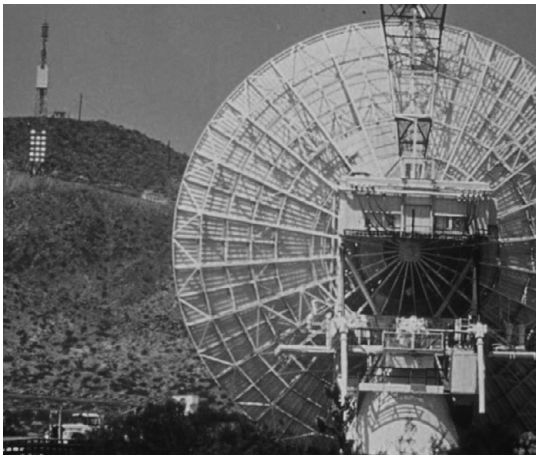

Figure 6.24 Wireless power transmission experiment at Venus JPL cite. ©1984 IEEE. Reprinted with permission from [126]

are embedded in circuits called rectifiers that are optimized in order to maximize the RF–dc conversion efficiency η_{RFdc}. One should note, however, that in principle nonlinear reactive elements could also be suitable for rectification provided they generate a required mixing product from RF to dc; however, we are not aware of any such examples to date.

The most commonly used diode-based rectifier topologies are the series or shunt diode rectifier, but also voltage doubler circuits with two diodes or bridge rectifier circuits with four diodes. These topologies are shown in Figure 6.26. Voltage multipliers with multiple diode stages such as the voltage doubler topology are also used in order to perform rectification as well as maximize the dc output voltage.

https://doi.org/10.1017/9781139600255.007 Published online by Cambridge University Press

Figure 6.25 Airplane powered by a microwave beam from a phased array antenna: (a) flight experiment, and (b) antenna array [178]. Photos courtesy of Prof. Naoki Shinohara, Kyoto University

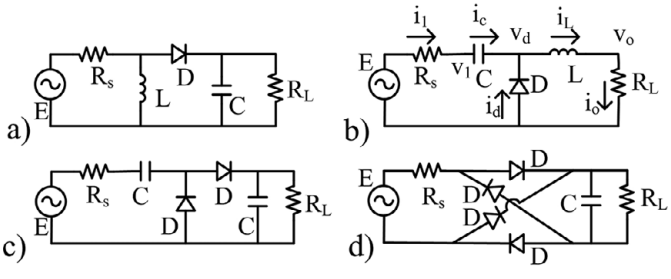

Figure 6.26 Diode rectifier topologies: (a) series, (b) shunt, (c) voltage doubler, and (d) bridge.

The nonlinear element acts as a switch, permitting current to flow through it only in one direction, and this functionality results in generating harmonics and dc power. In order to get a theoretical estimate of the maximum efficiency, one

https://doi.org/10.1017/9781139600255.007 Published online by Cambridge University Press

may proceed by considering an ideal switch with an "ON" state corresponding to a short circuit and an "OFF" state corresponding to an open circuit, taking care that the voltage and current values at the boundary of the two states must be the same. Then one applies Kirchhoff's laws and computes a time average of the voltage or current expressions over one period T of the RF signal. The results are used to derive an estimate of the RF–dc conversion efficiency. This methodology has been followed, for example, in [137, 180, 181]. More complicated models for the nonlinear device may be used by considering the nonlinear capacitance and series resistance of the diode [137] and nonideal open and short-circuit states for the switch [181]. Let us discuss the shunt diode rectifier following the approach by [180] considering an ideal switch model for the diode.

The available input power P_A, the dc output load power P_L, and the efficiency η_{RFdc} are

$$P_A = \frac{E^2}{8R_s} \tag{6.62}$$

$$P_L = \frac{V_o^2}{R_L} \tag{6.63}$$

$$n_{RFdc} = \frac{P_L}{P_A} = \frac{8R_s}{R_L}\left(\frac{V_o}{E}\right)^2. \tag{6.64}$$

We then proceed to write Kirchhoff's voltage law for the shunt rectifier circuit of Figure 6.26b:

$$v_1 + V_c = v_L + V_o = v_d, \tag{6.65}$$

where v_c and v_L is the voltage across the input capacitor C and output inductor L respectively. DC components are indicated by the capital V or I letters. It is assumed that the capacitor C has a sufficiently large value to present an RF short and that the inductor L has a sufficiently large value to present a dc short. Integrating over one period T, one obtains

$$\int_T v_1 dt + V_c T = \int_T v_L dt + V_o T \Rightarrow V_c = V_o. \tag{6.66}$$

The integral of the RF voltage across the inductor v_L vanishes since it presents a dc short. Furthermore, since no dc current flows through the resistor R_s (in the steady state) due to the dc blocking functionality of the capacitor C, the integral of v_1 also vanishes. Next we address the two states of the diode switch. Let us assume that the diode is in the "ON" state for a period $|t| < t_1$ and whereas the "OFF" state lasts from $t = t_1$ until $t = T - t_1$. In this case, during the "ON" state, one has

$$v_1(t) = -V_o \Rightarrow i_1(t)R_s = E\cos(\omega t) - V_o = E\cos(\omega t) - I_o R_L \tag{6.67}$$

and during the "OFF" state

$$i_1(t) = I_o \Rightarrow v_1(t) = E\cos(\omega t) - I_o R_s. \tag{6.68}$$

https://doi.org/10.1017/9781139600255.007 Published online by Cambridge University Press

We enforce the condition that $v(t_1)$ must take the same value for the two expressions for the "ON" and "OFF" states,

$$-V_o = E\cos(\phi) - I_o R_s \Rightarrow E\cos(\phi) = I_o(R_s - R_L), \tag{6.69}$$

where $\phi = \omega t_1$ and $V_o = I_o R_L$. Next, taking the integral of v_1 over a period T, one has

$$\int_T v_1 dt = 0 \Rightarrow \int_{-t1}^{t1} v_1 dt + \int_{t_1}^{T-t_1} v_1 dt = 0. \tag{6.70}$$

Using (6.67) for the first integral of the left-hand side and (6.68) for the second, one obtains

$$-V_o 2t_1 + \frac{E}{\omega}\left[\sin(\omega T - \omega t_1) - \sin(\omega t_1)\right] - I_o R_s(T - 2t_1) = 0. \tag{6.71}$$

Rearranging and using $V_o = I_o R_L$, $\omega T = 2\pi$ and $\phi = \omega t_1$,

$$E\sin(\phi) = -I_o\left[\phi R_L + (\pi - \phi)R_s\right]. \tag{6.72}$$

Combining (6.69) and (6.72) one obtains

$$\tan(\phi) - \phi = \frac{\pi R_s}{R_L - R_s} \Rightarrow \frac{R_L}{R_s} = \frac{\sin(\phi) + (\pi - \phi)\cos(\phi)}{\sin(\phi) - \phi\cos(\phi)}. \tag{6.73}$$

Using the preceding result in (6.69), one can compute the output voltage V_o

$$V_o = I_o R_L = \frac{R_L E\cos(\phi)}{R_s - R_L} = \frac{E}{\pi}\left[\sin(\phi) + (\pi - \phi)\cos(\phi)\right] \tag{6.74}$$

and the efficiency

$$\eta_A = \frac{8}{\pi^2}\left[\ sin(\phi) - \phi\cos(\phi)\right]\left[\sin(\phi) + (\pi - \phi)\cos(\phi)\right]. \tag{6.75}$$

It is easy to very if by substitution that the maximum efficiency is obtained for $\phi = \pi/2$, resulting in

$$\eta_{Amax} = \frac{8}{\pi^2} \approx 81.1\% \tag{6.76}$$

with $R_L = R_s$. It is interesting to note that the same maximum efficiency $\eta_{Amax} = 8/\pi^2 \approx 81.1\%$ for $R_L = R_s$ is obtained for the series rectifier too [180]. We will see in the next sections that it is possible to obtain 100% by properly terminating the harmonics generated by the rectifier.

6.6.1 Time Reversal Duality

Amplifier and rectifier circuits have an inverse functionality of converting dc electrical power to RF and the opposite respectively. Strictly speaking, an amplifier requires both a dc and an RF input and therefore oscillator circuits should be considered instead of amplifier circuits. However, let us disregard this fact for the sake of simplicity and consider both oscillator and amplifier as dc-to-RF conversion devices. Consideration of these properties has led to the formulation

https://doi.org/10.1017/9781139600255.007 Published online by Cambridge University Press

time reversal duality principle [182]. According to the time reversal duality principle, any resonant amplifier can be transformed to a resonant rectifier of the same operating class, with the nonlinear switching device current and voltage waveforms of the rectifier being time-reversed versions of the corresponding waveforms of the amplifier. In mathematical terminology, let us consider a dynamical system such as an oscillator or an amplifier described by the N-dimensional state vector $\mathbf{x}$, $\mathbf{x} \in \mathbf{R^N}$

$$\frac{d\mathbf{x}}{dt} = \mathbf{f}(\mathbf{x}(t), t), \tag{6.77}$$

where $\mathbf{f}$ is a nonlinear vector function. If one considers the reverse time variable $\tau = -t$, then

$$\frac{d\mathbf{x}}{d\tau} = -\mathbf{f}(\mathbf{x}(-\tau), -\tau). \tag{6.78}$$

One may consider (6.78) as a new dynamical system with state variables $\mathbf{y}$ in the forward time t [182] as

$$\frac{d\mathbf{y}}{dt} = \mathbf{g}(\mathbf{y}(t), t) \tag{6.79}$$

with $\mathbf{g} = -\mathbf{f}$ and $\mathbf{y}(t) = \mathbf{x}(-t)$. The equation $\mathbf{y}(t) = \mathbf{x}(-t)$ expresses precisely the fact that the state variables $\mathbf{y}$ of the second system are time-reversed versions of the state variables and $\mathbf{x}$ of the first system [182].

This has an important implication in wireless power transfer systems for the following reason. It is well known that there exist classes of switched power amplifier circuits that have a theoretical dc-to-RF efficiency of 100%, such as class-E, class-F, or class-F^{-1} [183]. The principle of operation of these classes is to design the voltage and current waveforms of the nonlinear switching device such that they are offset with each other so that their product, which corresponds to dissipated power, is equal to zero. The time reversal duality principle showed that one may design rectifier circuits based on the original amplifier circuits, having time-reversed voltage and current waveforms with respect to the original amplifier circuits and having theoretically 100% RF-to-dc conversion efficiencies.

Such rectifier circuits operating in GHz frequencies were successfully demonstrated in [181]. Specifically, a 2.14 GHz rectifier circuit based on a GaN HEMT class-F^{-1} amplifier had a power-added efficiency of 84% at an output power of 37.6 dBm. The rectifier had a measured RF–dc conversion efficiency of 85% for 10 W input power. A diode-based rectenna and active antenna oscillator circuit operating at microwave frequencies was reported in [184]. The rectenna was optimized to operate at 2.45 GHz with a high efficiency of 85% while as an oscillator the circuit was operating at 3.3 GHz with a low efficiency. This fact highlights the challenge in exploiting the time duality principle if one wants to design a circuit that operates both as a rectenna and as an active antenna oscillator. First, one has to tune both circuits to operate at the same frequency band, or in a more general concept at the desired operating bands as a rectenna

https://doi.org/10.1017/9781139600255.007 Published online by Cambridge University Press

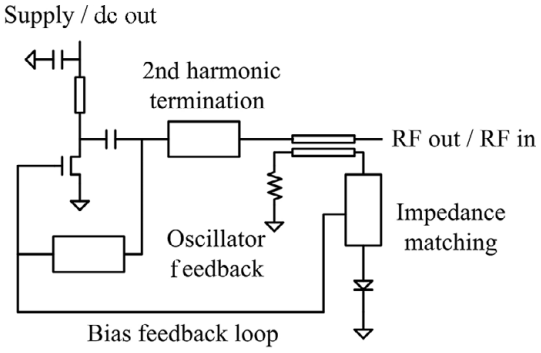

Figure 6.27 Schematic representation of a bidirectional rectifier and oscillator circuit operating at 2.45 GHz [185].

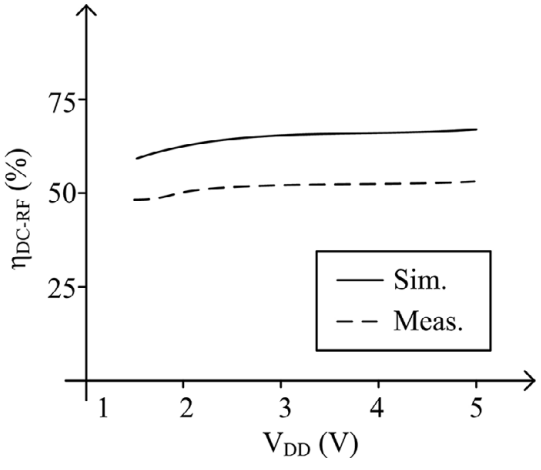

Figure 6.28 Performance of the oscillator mode of the circuit of Figure 6.27 [185].

and as an oscillator. Second, one has to tune both circuits to operate with high efficiency in both the rectenna mode and in the oscillator mode.

In [185], a transistor-based rectifier and oscillator circuit was designed operating at 2.45 GHz in both modes with an efficiency higher than 50%. A high-electron-mobility transistor (HEMT) device was used to implement the nonlinear circuits, and self-biasing of the gate of the device was explored in order to achieve a high efficiency at the oscillating mode. The circuit is shown in Figure 6.27 and the performance as an oscillator and as a rectifier is shown in Figures 6.28 and 6.29 respectively.

https://doi.org/10.1017/9781139600255.007 Published online by Cambridge University Press

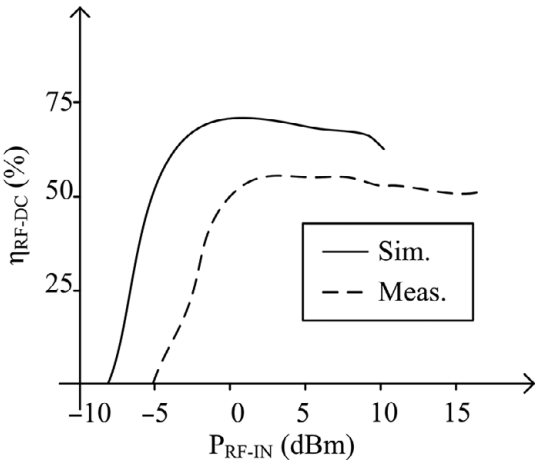

Figure 6.29 Performance of the rectifier mode of the circuit of Figure 6.27 [185].

6.7 Far-Field Wireless Power Transmission at Millimeter Wave Frequencies and Beyond

While the majority of far-field wireless power transmission circuits have been in the low GHz range due to the fact that it is easier and cheaper to generate high power and to obtain high-efficiency rectifiers at these lower microwave frequencies, operation at higher frequencies such as millimeter waves also has certain advantages.

Millimeter wave circuits allow for a small form factor due to the small wavelength, and therefore they permit the design of very compact circuits. More importantly, for the same reason they enable the implementation of a very large number of antenna elements, thus allowing one to design a very directive power transmitting antenna on one hand and a very directive receiving antenna or a large receiving surface of many individual subarray rectennas on the other hand. Therefore, it is possible to have a better control of the directive transmission of power and to minimize unwanted power transmission at undesired directions. These advantages may outweigh the high cost and less favorable performance of the available nonlinear devices in these frequencies.

Selected examples of millimeter wave far-field wireless power transmission circuits and systems include, for example, a 94 GHz rectenna array by JPL [186], and Class-F millimeter wave rectennas operating at 24 GHz and 60 GHz [142]. An example of a 24 GHz rectenna implemented in substrate integrated waveguide technology is shown in Figure 6.30 [187]. Its efficiency is shown in Figure 6.31, where one can verify that it is more difficult to obtain a high efficiency at comparable power levels at millimeter waves in comparison with rectennas operating at low GHz.

https://doi.org/10.1017/9781139600255.007 Published online by Cambridge University Press

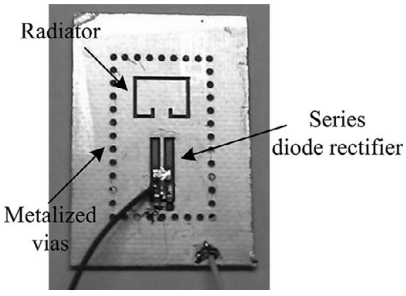

Figure 6.30 24 GHz SIW rectenna prototype. ©2013 IEEE. Reprinted with permission from [187]

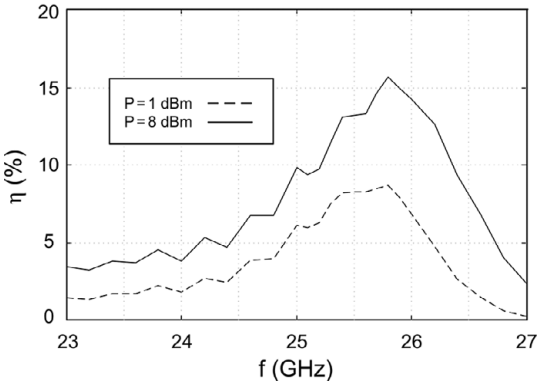

Figure 6.31 24 GHz SIW rectenna measured efficiency [187].

While high power generation is challenging at millimeter wave and toward THz frequencies, high power and highly directive optical sources are much easier to implement using lasers. Consequently, laser power transmission presents another exciting possibility for powering wirelessly devices. There have been successful demonstrations of transmitting power to a small aircraft using a laser, where solar cells have been used to receive the laser beam and convert it to electrical power [188].

6.8 Problems and Questions

1. What is the difference between inductive coupling and resonant inductive coupling?
2. Calculate the power transfer efficiency of a resonant inductive coupling system with $L_1 = L_2 = 5$ μH, $k = 0.3$ and $R_{load} = 100$ Ω operating at 13.56 MHz. Assume that the two coils have resistances $R_1 = R_2 = 2$ Ω.

https://doi.org/10.1017/9781139600255.007 Published online by Cambridge University Press

3. Calculate the number of turns necessary to synthesize an inductance of 0.1 μH with a square printed coil with side length $D = 2$ cm using the modified Wheeler formula (assume $K_1 = 2.34$ and $K_2 = 2.75$).
4. Calculate the optimum value of the load resistance R_{load} for a nonresonant inductive coupling system with $L_1 = L_2 = 20$ μH and $k = 0.2$ at 13.56 MHz. Assume that the two coils have resistances $R_1 = R_2 = 2$ Ω.
5. Compute the maximum theoretical efficiency of a series diode rectifier with the circuit diagram shown in Figure 6.26.
6. Compute the maximum theoretical efficiency of a voltage doubler with the circuit diagram shown in Figure 6.26.
7. Compute an approximate solution for the eigenvalues of a three coil system with characteristic equation (6.55) as a perturbation of the solution obtained by setting $2k_{12}k_{23}k_{13} \approx 0$.

https://doi.org/10.1017/9781139600255.007 Published online by Cambridge University Press